Heterogeneous Reaction of NO_2: Characterization of Gas-Phase and Adsorbed Products from the Reaction, $2NO_2(g) + H_2O(a) \rightarrow HONO(g) + HNO_3(a)$ on Hydrated Silica Particles

A. L. Goodman, G. M. Underwood, and V. H. Grassian*

Department of Chemistry and Center for Global and Regional Environmental Research, University of Iowa, Iowa City, Iowa 52242

Received: March 26, 1999; In Final Form: July 15, 1999

This study provides the first in-situ characterization of the products in the heterogeneous reaction $2NO_2(g) + H_2O(a) \rightarrow HONO(g) + HNO_3(a)$. Transmission FT-IR spectroscopy and UV−vis spectroscopy were used to probe the heterogeneous chemistry of gas-phase nitrogen dioxide on hydrated SiO_2 particles. At 298 K, gaseous nitrogen dioxide reacts with adsorbed water on the surface of SiO_2 particles to form adsorbed nitric acid and gas-phase nitrous acid. FT-IR spectroscopy of the hydrated SiO_2 surface following reaction with NO_2 provides definitive identification of the adsorbed nitric acid product. The reaction does not occur when gas-phase nitrogen dioxide is reacted on dehydrated silica particles. The gas-phase product nitrous acid was detected with both FT-IR and UV−vis spectroscopy. Although homogeneous and heterogeneous reactions can contribute to the observed HONO signal, flow cell measurements can be used to distinguish between heterogeneous and homogeneous reaction pathways leading to HONO production.

Introduction

Hydroxyl radical is the most important trace species in atmospheric oxidation mechanisms.[1,2] While it is clear that O_3 photolysis is the main source of OH radicals in the stratosphere, mechanisms for OH radical formation in the troposphere are still being debated. One source of hydroxyl radical is from the photodissociation of nitrous acid (HONO), as HONO undergoes photolysis at wavelengths between 330 and 380 nm.[3]

$$HONO + h\nu \rightarrow OH + NO \quad (1)$$

Although HONO concentrations up to 14 ppb have been observed in polluted urban environments, HONO formation is not well understood.[4,5] Lee and Schwartz have shown that reactions 2 and 3 are too slow in the gas and aqueous phases to be relevant under atmospheric conditions.[6]

$$NO_2 + NO + H_2O \rightarrow 2HONO \quad (2)$$

$$2NO_2 + H_2O \rightarrow HONO + HNO_3 \quad (3)$$

Evidence suggests, however, that these reactions may occur at a faster rate by a heterogeneous or surface-catalyzed mechanism.[7−19] In fact, surface reactions may be responsible for as much as 95% of all the HONO found in the troposphere.[9−11] A recent review article discusses the evidence presented for heterogeneous reaction of NO_2 to produce gas-phase HONO in humid environments.[12] The reaction proceeds over a wide variety of surfaces including those of glass, sodium halides, metals, and metal oxides.

Several laboratory studies have reported that heterogeneous HONO formation via reaction 3 is first order in both NO_2 and H_2O,[9−12,18]

$$d[HONO]/dt = k[NO_2][H_2O] \quad (4)$$

with the rate-limiting step being adsorption of NO_2. Using environmental chambers containing NO_2 and H_2O, Sakamaki et al. and Pitts et al. proposed that reaction 3 provides the best model of the data for the heterogeneous formation of HONO, although no HNO_3 was directly detected.[8,9] Therefore, without full characterization of all of the reactants and products in reaction 3, the reaction has been considered somewhat speculative.[18] The lack of any observable HNO_3 in the gas phase has been explained by the suggestion that it sticks to the walls of the environmental chamber. This suggestion is supported in some recent experiments in which HNO_3 was detected via ex situ measurements.[17,19]

As mineral dust has been proposed to be an important reactive surface in the global troposphere,[20−22] we have begun a comprehensive study to probe potentially important heterogeneous reactions of trace atmospheric gases such as NO_2 on mineral oxide particles.[23−25] In our previous work,[25] it was shown that NO_2 reacts with dehydrated and hydrated Al_2O_3, Fe_2O_3, and TiO_2 particles to form surface nitrite at low NO_2 exposures and surface nitrate at high NO_2 exposures.[24−26] Gas-phase NO is produced in the reaction as well. It is important to note that adsorbed water is not needed for reaction of NO_2 to occur on Al_2O_3, Fe_2O_3, and TiO_2 particles.

In this study, in-situ spectroscopic probes were used to investigate the heterogeneous reaction of gas-phase NO_2 with water adsorbed on the surface of SiO_2 particles at 298 K. As discussed below, little reaction occurs between gaseous nitrogen dioxide and SiO_2 particles that have been dehydrated. However, reaction of gas-phase NO_2 with water adsorbed on the SiO_2 particles results in the formation of gas-phase nitrous acid and surface-bound nitric acid according to reaction 3. This study shows that spectroscopic techniques that probe the reactive particle surface can be useful in providing mechanistic information about potentially important heterogeneous tropospheric reactions.

In addition, a flow reactor coupled to a quadrupole mass spectrometer, operated both at pressures above and in the molecular flow regime, was used to investigate contributions

* To whom correspondence should be addressed.

10.1021/jp9910688 CCC: $18.00
Published on Web 08/20/1999

to HONO production due to homogeneous reaction of NO_2. In the molecular flow regime there are essentially no collisions between gas-phase molecules and, therefore, only heterogeneous reactions can contribute to the production of HONO. At pressures above the molecular flow regime, collisions between gas-phase molecules are more likely and thus there is the possibility that a homogeneous reaction pathway can contribute to the formation of gas-phase HONO. In cases where homogeneous and heterogeneous chemistry occurred, HONO produced from homogeneous reactions could be accounted for.

Experimental Section

Commercially available SiO_2 (Aerosil 200, Degussa) particles were used in this study. The particles are nearly spherical with an average particle diameter of 20 nm as measured with transmission electron microscopy and have a surface area of 226 m^2/g as measured by BET analysis. For FT-IR measurements, SiO_2 samples were prepared by spraying a water slurry of the oxide powder onto one-half of a tungsten grid (Buckbee Mears, 100 lines per inch tungsten mesh wire widths of 0.0015″ and thickness of 0.002″). The other half of the tungsten grid was left blank for gas-phase measurements. Approximately 33 mg of SiO_2 was sprayed onto a 3 cm × 1 cm area of the grid giving a sample thickness of ~0.5 mm. The tungsten grid containing the oxide sample was held in place by a set of Ni jaws inside of the IR cell. The sample can be resistively heated to desired temperatures.

The IR cell is made of a stainless steel cube with BaF_2 windows and is attached to a gas manifold through a bellows hose. The total volume of the IR cell and bellows hose is 400 mL. The manifold consists of a turbomolecular pump, absolute pressure transducer (range 0.001 to 10.000 Torr), and a port for gas introduction. After the tungsten grid supporting the silica was placed into the IR cell, the system was evacuated from atmosphere to $\sim 10^{-5}$ Torr.

The IR cell is mounted on a linear translator inside the FT-IR spectrometer (Mattson Instruments) so that both halves of the grid can be measured by simply moving the cell through the IR beam path. Typically, 250 scans were acquired at an instrument resolution of 4 cm^{-1}. The low-frequency cutoff of the SiO_2 spectra near 1300 cm^{-1} is due to strong lattice oxide absorptions.

A UV−vis spectrometer (PE Lambda 20) was used to measure gas-phase spectra in a quartz cuvette with a path length of 1 cm. Transmittance spectra ($\%T = T/T_0$) were recorded, using the evacuated cuvette as the background, T_0, and a cuvette containing reactant gases and ~16 mg of SiO_2 powder placed on the bottom of the cuvette as the sample, T.

A flow cell reactor coupled to a quadrupole mass spectrometer (UTI, DetecTorr II) that could be operated at both pressures above and in the molecular flow regime was used to investigate homogeneous and heterogeneous contributions to gas-phase product formation. The mass spectrometer is housed in a vacuum chamber equipped with a 400 L/s ion pump and an ion gauge (both from Varian). The region between the quadrupole mass spectrometer and the flow reactor is pumped by a 100 L/s turbomolecular pump for differential pumping of the mass spectrometer.

The flow cell reactor consists of a stainless steel reducing cross with a sample holder attached to the bottom flange. The sample holder and the inside of the cover for the sample were both coated with Halocarbon Wax series 1500 to provide a chemically inert surface. Samples for the Knudsen cell were loaded onto the bottom of the sample holder and spread so that the bottom of the sample holder was covered evenly with the silica powder (~100 mg). The sample was then pressed down to form a flat surface within the sample holder. The powdered sample was covered by a blank flange attached to a linear translator. The seal between the sample holder and the cover was made with a viton O-ring. Prior to each experiment, the reactor was passivated by flowing NO_2 through for approximately 90 min. During passivation the SiO_2 particles were sealed with the blank flange.

NO_2 (Matheson, 99.95% purity) was used as supplied. Distilled H_2O (Milli-Q) was degassed prior to use. D_2O (Alfa Aesar, 99.8% isotopic) was used as supplied. Gaseous HNO_3 acid was taken from a 1:3 mixture of concentrated HNO_3 (70.6% HNO_3, Mallinckrodt) and H_2SO_4 (95.9% H_2SO_4, Mallinckrodt).

Results and Discussion

Transmission FT-IR Spectroscopy of SiO_2 Particles with Different Amounts of Adsorbed H_2O. Reaction of gaseous NO_2 on SiO_2 particles with varying amounts of adsorbed water was investigated using transmission FT-IR spectroscopy (vide infra). For experiments on samples labeled dehydrated SiO_2, the particles were heated to 673 K to remove all adsorbed water and some surface hydroxyl groups as determined by FT-IR spectroscopy. For experiments on samples labeled hydrated SiO_2, the particles were exposed to at least 10 Torr of H_2O and subsequently evacuated to pressures on the order of 1×10^{-4} Torr. By pumping out the water vapor, the only source of water for reaction 3 is that which is adsorbed on the surface of the SiO_2 particles.

Representative FT-IR spectra in the spectral region extending from 1300 to 4000 cm^{-1} of SiO_2 particles with varying amounts of adsorbed water on the surface of the particles are shown in Figure 1. These absorbance spectra were made by referencing the SiO_2 spectrum to that of the blank grid. Assignments of the spectral features present in the SiO_2 spectrum are indicated in Figure 1.[26] Changes in the OH stretching mode region are clearly observed for dehydrated SiO_2 particles, hydrated SiO_2 particles, and SiO_2 particles in the presence of gas-phase water corresponding to 4% RH. As can be seen in the spectra, there is enhanced intensity in the region corresponding to the OH stretching motion of associated (hydrogen bonded) hydroxyl groups and adsorbed water for the hydrated SiO_2 particles and for SiO_2 particles in the presence of gas-phase H_2O compared to the spectrum of dehydrated SiO_2 particles. Also shown in Figure 1 is the spectrum of a deuterated SiO_2 sample where surface hydroxyl groups and adsorbed water were exchanged with deuterated water.

The SiO_2 particles labeled dehydrated, hydrated, and 4% RH correspond to particles with surfaces that have different amounts of adsorbed water. To quantify the coverage of water on these particle surfaces, a calibration was done using the adsorption/desorption data of Sneh et al. for H_2O on a fully hydroxylated SiO_2 surface.[27] In that work, it was determined that at ambient temperatures (298 K) the SiO_2 surface would be completely covered with one layer of adsorbed water at 10% RH. Water coverages in this study were then determined by assuming that one layer of water covered the SiO_2 particle surface at 10% relative humidity. FT-IR spectra were collected for SiO_2 particles at water pressures corresponding to 10% RH as well as other water pressures. Water coverages could then be scaled appropriately to the 10% RH data. Because the OH stretching region contains contributions from associated hydroxyl groups whose contribution to the band cannot simply be subtracted out, the scaling factor was determined from a plot of the integrated

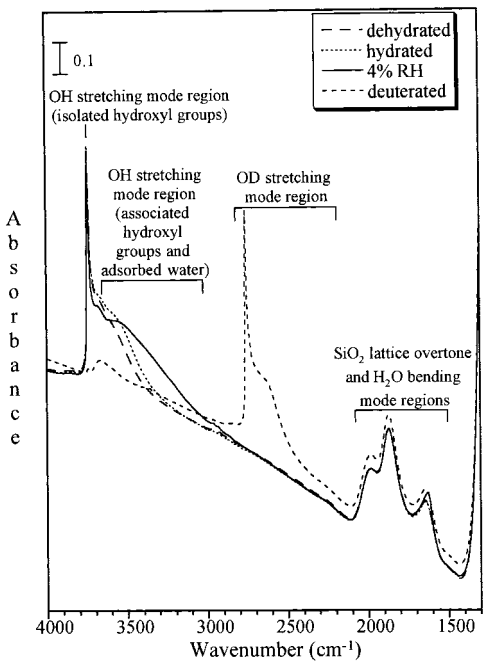

Figure 1. Transmission FT-IR spectra of SiO_2 particles that differ in H_2O (D_2O) coverages. For samples labeled dehydrated SiO_2, the particles were heated to 673 K to remove all adsorbed water and some surface hydroxyl groups. For samples labeled hydrated SiO_2, the particles were exposed to at least 10 Torr of H_2O and subsequently evacuated to pressures on the order of 1×10^{-4} Torr. For samples labeled 4% RH SiO_2, the particles were in equilibrium with gas-phase water corresponding to a relative humidity of 4%. For samples labeled deuterated SiO_2, the hydroxyl groups and adsorbed water were exchanged with D_2O.

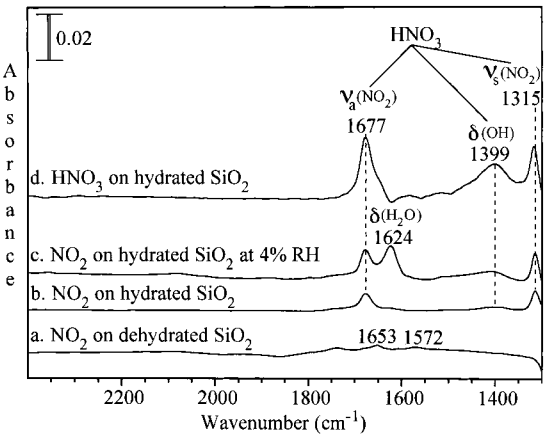

Figure 2. Transmission FT-IR spectra of adsorbed products on SiO_2 following reaction of gas-phase NO_2 on SiO_2. FT-IR spectra of adsorbed products were recorded in the presence of the gas phase; however, gas-phase absorptions were subtracted from each of the spectra: (a) FT-IR spectrum of dehydrated SiO_2 in the presence of NO_2 (663 mTorr); (b) FT-IR spectrum of hydrated SiO_2 in the presence of NO_2 (625 mTorr); (c) FT-IR spectrum of hydrated SiO_2 in the presence of NO_2 (625 mTorr) and gas-phase H_2O (4% RH). (d) FT-IR spectrum of an authentic sample of HNO_3 adsorbed on hydrated SiO_2.

TABLE 1: Surface Product Characterization: Vibrational Assignment of HNO_3 Adsorbed on SiO_2

mode description[a]	gas-phase HNO_3 (DNO_3)	adsorbed[b] HNO_3 (DNO_3)
ν(OH)	3551[c] (2622)	*d*
$\nu_a(NO_2)$	1708 (1687)	1677 (1632)
δ(OH)	1331 (1014)	1399 (n.o.[e])
$\nu_s(NO_2)$	1325 (1308)	1315 (1320)
t(NO_2)	879 (888)	n.o.
$\omega(NO_2)$	762 (763)	n.o.
ν(NO)	647 (641)	n.o.
$\rho(NO_2)$	579 (541)	n.o.
τ(HONO)	456 (342)	n.o.

[a] Mode description (Shimanouchi, 1977). [b] This work. [c] Frequencies in cm^{-1}. [d] Due to hydrogen bonding interactions between adsorbed nitric acid and water, the OH (OD) stretching region was quite broad and not easily assigned to a single band (see text for further discussion). [e] n.o. = not observed, below SiO_2 lattice absorptions.

area of the water bending mode (1624 cm^{-1}). Although the bending mode region also contains SiO_2 lattice overtone modes, these can be subtracted out using a dehydrated SiO_2 spectrum as these modes are not affected by the presence of water on the surface of the particle. Using this calibration procedure, the SiO_2 particles labeled dehydrated, hydrated, and 4% RH were determined to have water coverages of <0.01, 0.08, and 0.6 monolayers, respectively.

Transmission FT-IR Spectroscopy and UV−Vis Spectroscopy of Surface Reactions of NO_2 on SiO_2. In these experiments, a known pressure of NO_2 was admitted into the IR cell containing SiO_2 particles. When the gas reached an equilibrium pressure, two spectra were recorded; one of the gas phase and the other of the surface in the presence of the gas. Absorbance spectra of surface species only were first obtained by referencing a SiO_2 sample spectrum after reaction to a SiO_2 spectrum prior to reaction. This gave a spectrum that showed changes that occur to the silica surface and the gas phase after reaction. Gas-phase absorption bands measured through the blank grid that contained no SiO_2 could then be spectrally subtracted in order to obtain a spectrum of surface species only.

Upon exposure of dehydrated SiO_2 to NO_2, two weak bands with frequencies of 1653 and 1572 cm^{-1} appear in the SiO_2 spectra (Figure 2a). These bands are in the expected region for oxide-coordinated surface nitrate. Similar, but much more intense, bands are observed when NO_2 reacts with metal oxides such as Al_2O_3 and TiO_2 to form surface nitrate.[23−25] The intensity of these bands are quite weak in the SiO_2 spectrum and show that formation of oxide-coordinated nitrate occurs much less readily on SiO_2 as compared to Al_2O_3 and TiO_2.

When NO_2 is added to the infrared cell containing hydrated silica with a surface coverage of approximately 0.08 monolayers of adsorbed water, absorption bands appear in the silica spectrum at 1677, 1399, and 1315 cm^{-1} (Figure 2b). As discussed below, these bands can be assigned to the vibrational modes of adsorbed HNO_3. In the presence of gas-phase water at a relative humidity (RH) of 4%, the bands assigned to HNO_3 increase in intensity, and an increase in intensity of the bending mode of adsorbed water at 1624 cm^{-1} (Figure 2c) is also observed. The assignment of the bands to adsorbed HNO_3 is confirmed by the spectrum of an authentic sample of HNO_3 adsorbed on SiO_2 (Figure 1d). The three bands in the spectrum can be assigned to $\nu_a(NO_2)$, 1677 cm^{-1}; δ(OH), 1399 cm^{-1}; and $\nu_s(NO_2)$, 1315 cm^{-1} modes of adsorbed HNO_3 (Table 1). As seen in Table 1, these bands are shifted by 10−68 cm^{-1} from the gas-phase HNO_3 frequencies,[28] but compare well to the infrared spectrum of HNO_3 in highly concentrated aqueous solution which has absorptions at 1670 and 1300 cm^{-1} that are assigned to the $\nu_a(NO_2)$ and $\nu_s(NO_2)$ modes, respectively.[29] The OH stretching region (not shown) is complicated and showed an intense broad absorption band extending from 3700 to as low as 2700 cm^{-1}. This broad band is most likely due to hydrogen bonding interaction between HNO_3 and H_2O. Further studies are currently underway to more

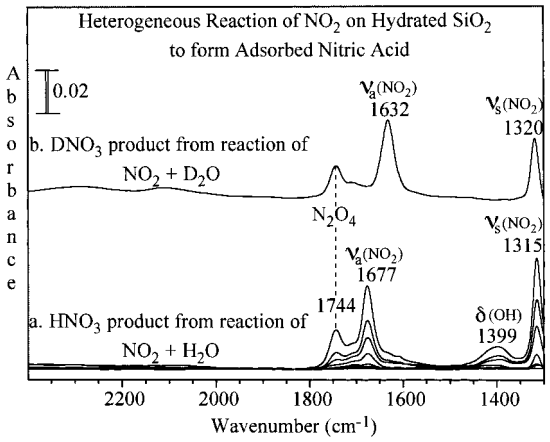

Figure 3. (a) FT-IR spectra of hydrated SiO_2 recorded as a function of NO_2 pressure (0.058, 0.117, 0.237, 0.625, 1.318, 2.011, and 3.417 Torr). (b) FT-IR spectrum recorded following reaction of NO_2 (1.318 Torr) on SiO_2 in which adsorbed H_2O had been exchanged with D_2O.

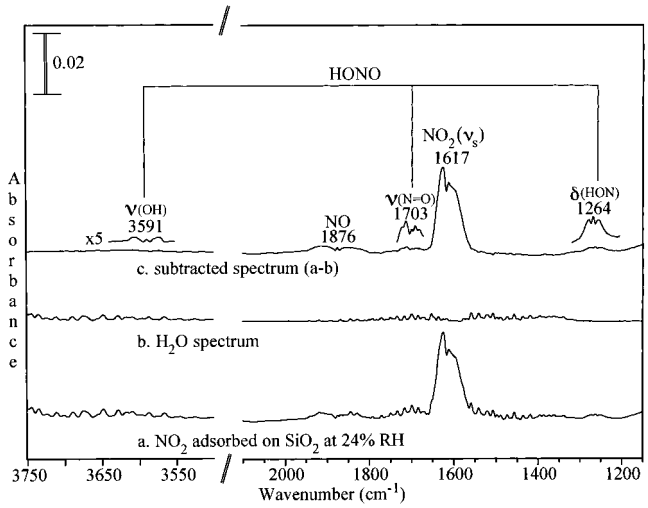

Figure 4. (a) FT-IR spectrum of the gas phase after reaction of NO_2 (3.404 Torr) with hydrated SiO_2 in the presence of H_2O vapor (24% RH). (b) FT-IR spectrum of gas-phase H_2O. (c) Difference spectrum (a − b) to remove H_2O bands from spectrum a is shown. Absorptions due to *trans*-HONO, NO_2, and NO are present in the spectrum (3591, 1703, and 1264 cm^{-1}, HONO; 1617 cm^{-1}, NO_2; 1876 cm^{-1}, NO).

clearly understand the adsorption of HNO_3 on hydrated SiO_2 and other hydrated oxide particles.

The reaction of NO_2 on hydrated SiO_2 was investigated as a function of NO_2 pressure (Figure 3a). NO_2 pressures ranged from 58 mTorr to 3.4 Torr. At the lower pressures, absorptions at 1677, 1399, and 1315 cm^{-1} due to adsorbed HNO_3 grow as the pressure increases. At the higher pressures, bands at 1744 and 1265 cm^{-1} are apparent in the spectrum and are assigned to the asymmetric and symmetric stretch, respectively, of the NO_2 dimer, N_2O_4. The symmetric stretch of N_2O_4 at 1265 cm^{-1} is not shown in Figure 3a because this band coincides with the steep background in this region due to SiO_2 lattice absorptions. At equilibrium, the N_2O_4/NO_2 ratio is 5% at 3.4 Torr and the frequencies of the vibrational modes of adsorbed N_2O_4 bands are in close agreement to the gas-phase values of 1758 and 1264 cm^{-1}.[30] Therefore, it is reasonable to assign these bands at 1744 and 1265 cm^{-1} to adsorbed N_2O_4.

In another experiment done to confirm that gas-phase NO_2 reacts with surface adsorbed water, NO_2 was reacted on a SiO_2 sample in which surface hydroxyls and adsorbed water were exchanged with D_2O. FT-IR spectroscopy was used to monitor the depletion of the OH and H_2O absorptions (3200−3600 cm^{-1}) concurrent with the growth of OD and D_2O absorptions (2400−2750 cm^{-1}) during the exchange process. The infrared spectrum recorded after SiO_2 particles with adsorbed D_2O were exposed to NO_2 is shown in Figure 3b. Only two bands were apparent in the spectrum, these two bands are assigned to the $\nu_a(NO_2)$ mode at 1632 cm^{-1} and $\nu_s(NO_2)$ mode at 1320 cm^{-1} of adsorbed DNO_3. As expected, these two modes shifted only slightly in frequency from HNO_3, whereas the frequency of the bending mode, σ(OD), of DNO_3 is significantly shifted from the 1399 cm^{-1} δ(OH) mode of HNO_3.[28] On the basis of the isotope effect, the frequency of the O−D bending mode is expected to be near 990 cm^{-1} but is not observed because of strong SiO_2 lattice absorptions below 1300 cm^{-1} (see Table 1). Thus, the infrared data clearly demonstrate that in the presence of gas-phase NO_2 water adsorbed on the silica particles can react to form adsorbed HNO_3.

The FT-IR spectra shown for surface-bound species were recorded in the presence of the gas phase. Upon evacuation of the gas-phase, however, the FT-IR spectrum shows that HNO_3 slowly desorbs from the surface. However, the two weak bands at 1653 and 1572 cm^{-1} remain in the spectrum, as discussed (vide supra), these bands can be assigned to the formation of small amounts of oxide-coordinated surface nitrate[25] on the silica particle.

According to reaction 3, the production of gas-phase HONO is also expected from the heterogeneous reaction of NO_2 on hydrated SiO_2 particles. The gas-phase spectrum obtained by reacting NO_2 on hydrated SiO_2 followed by the addition of gas-phase water at a relative humidity (RH) of 24% is shown in Figure 4a. Because absorption bands of water overlap the region where HONO bands are expected, a water spectrum, as shown in Figure 4b, was subtracted from the spectrum shown in Figure 4a. In the difference spectrum, Figure 4c, bands at 3591, 1703, and 1264 cm^{-1} became apparent. On the basis of literature assignments, the bands at 3591, 1703, and 1264 cm^{-1} are assigned to the ν(OH), ν(N═O), and δ(HON) modes, respectively, of gas-phase *trans*-HONO.[31] In these experiments, NO is also present in the spectrum at 1876 cm^{-1}. Sakamaki et al. and Pitts et al. also reported NO production and suggested that NO may come from wall reactions of HONO.[8,9] In other experiments, we have observed some NO production from wall reactions of NO_2 as well.

Further evidence for the formation of gas-phase HONO in the presence of hydrated SiO_2 is presented in Figure 5. Transmission UV−vis spectroscopy was used to further corroborate the FT-IR results for HONO formation because HONO absorbs strongly in the UV between 310 and 390 nm.[19] Although NO_2 absorbs in the same region as HONO, the HONO features can be easily discerned. The two spectra shown in Figure 5 were obtained by reacting NO_2 and H_2O in a quartz cuvette that did not contain SiO_2 and in a quartz cuvette containing approximately 16 mg of SiO_2. Absorptions due to HONO are seen in both cases; however, in the case where SiO_2 is present, there is significantly more HONO produced. Without the silica present, reaction 3 is most likely catalyzed by the walls of the cuvette. However, as discussed below, there may also be contributions from homogeneous gas-phase reactions to HONO formation.

Flow Cell Measurements of the NO_2 + H_2O Reaction. Flow cell measurements provided additional insight into the reaction of NO_2 and H_2O. In these experiments, gas-phase pressures of reactants were measured with an absolute pressure

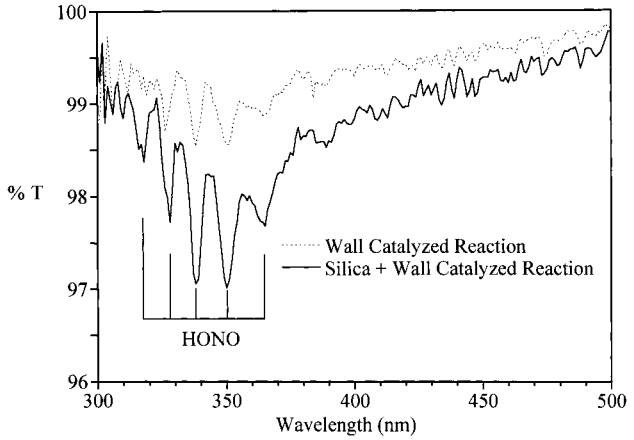

Figure 5. UV−vis spectra following reaction of NO_2 and H_2O shows absorptions due to gas-phase HONO. The wall-catalyzed spectrum was obtained by reacting NO_2 (3.0 Torr) with H_2O (10.0 Torr). The silica + wall catalyzed spectrum was obtained by reacting NO_2 (3.0 Torr) with H_2O (10.0 Torr) in the presence of 16 mg of hydrated SiO_2.

transducer that could read down to 1×10^{-6} Torr. The SiO_2 particles were covered with a lid while a steady-state flow of NO_2 through a 0.0204 cm^2 aperture to the mass spectrometer was established. With this experimental arrangement, the escape rate constant, k_{esc}, for a gas of molecular weight, M, is equal to 3.2×10^{-14} $kg^{1/2}$ s^{-1} $[M]^{-1/2}$. Once steady-state flow was reached, the lid was then opened to expose the particles to the gas. The design of the flow cell is such that the volume of the cell changes very little, <0.5%, when the SiO_2 particles are exposed. Therefore, no volume corrections need to be made to the data.

Flow cell measurements were first carried out in the absence of SiO_2 particles. In this case, the stainless steel walls of the reactor provided a surface for heterogeneous chemistry. Initially, a steady-state flow of NO_2 of $\sim 1 \times 10^{15}$ molecules s^{-1} was established (see Figure 6). Water was then introduced into the reactor at various pressures. The total pressure in the reactor is the sum of the partial pressures of reactants and products which can be approximated to be the sum of the NO_2 and H_2O pressures. Therefore, the total pressure in the reactor is predominantly due to gas-phase water, and the flow of water varied from 7×10^{15} to 3×10^{16} molecules s^{-1}. The molecular flow regime, where gas-phase collisions are negligible is indicated in the figure. Thus, conditions in the flow cell varied such that both heterogeneous and homogeneous chemistry could occur for conditions above the molecular flow regime, whereas only heterogeneous chemistry dominates in the molecular flow regime.

Gas-phase product formation[32,33] shows contributions from both homogeneous and heterogeneous reaction pathways. It can be seen from the data presented in Figure 6 that gas-phase HONO is produced under all conditions, i.e., when the pressure in the reactor is both above and in the molecular flow regime. In contrast, gas-phase HNO_3 is only produced when the total pressure is above the molecular flow regime. The two double-headed arrows in Figure 6 point to conditions in the reactor corresponding to the molecular flow regime. It can be seen that gas-phase HONO is produced under these conditions, whereas gas-phase HNO_3 is not. These data show that gas-phase HONO is formed from heterogeneous reaction of NO_2 and H_2O on the stainless steel walls of the reactor whereas HNO_3 remains adsorbed on the walls, in agreement with the FT-IR data presented here. At pressures above the molecular flow regime, both gas-phase HONO and HNO_3 are produced. These data

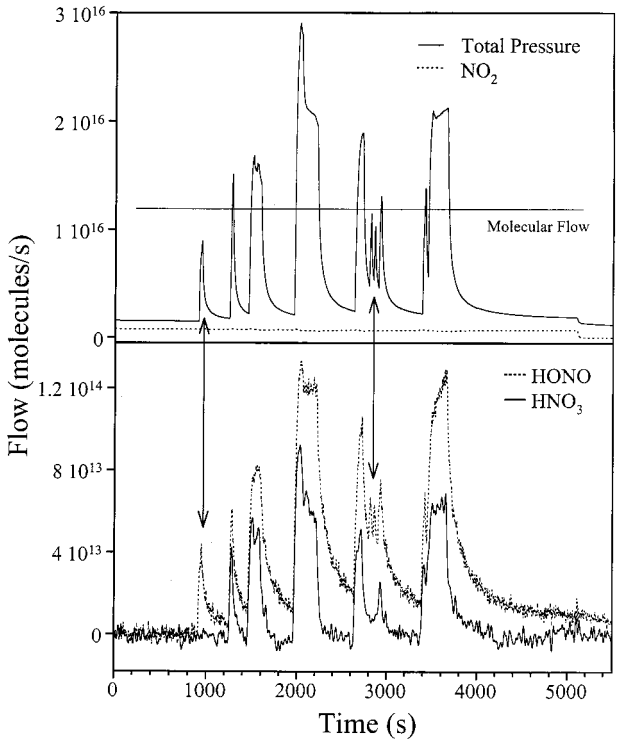

Figure 6. Flow cell reactor mass spectral data for reaction of NO_2 in the absence of SiO_2 particles. In these experiments, steady-state flow of NO_2 of $\sim 1 \times 10^{15}$ molecules s^{-1} was established. Water was then introduced into the flow cell at various pressures. The flow, corresponding to a total pressure, P, in the reactor is plotted in the figure and is approximated to be the sum of NO_2 and H_2O in the reactor. The molecular flow regime, where there are no gas-phase collisions, is below 1.2×10^{16} molecules s^{-1}. The water flow varied from 7×10^{15} to 3×10^{16} molecules s^{-1}; that is, conditions in the reactor were above and in the molecular flow regime. Gas-phase products, HNO_3 and HONO, were detected and show contributions from both homogeneous and heterogeneous reaction pathways (see text for details).

suggest that gas-phase HNO_3 is produced from a homogeneous reaction and that heterogeneous and homogeneous reactions contribute to HONO formation in the gas phase. Alternatively, gas-phase HNO_3 may be due to desorption from the walls as the wall surface saturates with HNO_3 at the higher pressures and thus higher reaction rates.

Flow cell measurements were then carried out on SiO_2 particles that contained different amounts of adsorbed water. SiO_2 particles evacuated overnight to a pressure of $<1 \times 10^{-6}$ Torr (labeled dehydrated SiO_2) showed no measurable loss of NO_2 from the gas phase, as seen in Figure 7. SiO_2 particles evacuated for shorter periods of time did show a measurable amount of NO_2 uptake. Data are presented in Figure 7 for SiO_2 particles that were exposed to 10 Torr of water at 298 K followed by evacuation for 20 min. There was a decrease in NO_2 flow rate and reaction on hydrated SiO_2 particles when the lid was open. There is an initial spike in the NO_2 flow rate, but then the flow rate approaches the steady-state value. The lid was closed again for 300 s, and subsequently the oxide particles were exposed. The second time the lid was open there was less of a decrease in the NO_2 signal.

The H_2O flow rate for the two SiO_2 samples, dehydrated and hydrated, is also shown in Figure 7. The H_2O signal increases when the lid is open, indicating that water is outgassing from the SiO_2 sample. There are several points that can be made concerning the H_2O desorption from the SiO_2 samples. First, the amount of water coming from the SiO_2 sample labeled dehydrated is a factor of 100 times less than the SiO_2 sample

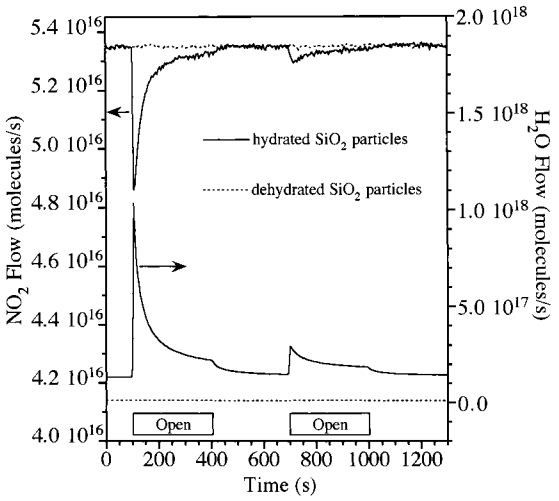

Figure 7. Flow cell reactor mass spectral data for reaction of NO_2 on SiO_2. The flow rate in molecules per second is shown for two gas-phase molecules, NO_2 (scale for NO_2 flow is shown on the *y*-axis on the left) and H_2O (scale for H_2O flow is shown on the *y*-axis on the right), during reaction on dehydrated and hydrated SiO_2. At time $t =$ 100 s, the sample holder is opened and there is a drop in the NO_2 flow rate as NO_2 reacts on the surface of hydrated SiO_2 particles (i.e., particles exposed to 10 Torr H_2O overnight and evacuated for 20 min) but not dehydrated SiO_2 particles (i.e., particles evacuated overnight). The sample holder is then closed and the NO_2 signal returns to its baseline value. The process of exposing the surface to NO_2 was repeated once again. The plot also shows that there is a significant amount of water outgassing from the hydrated but not the dehydrated sample.

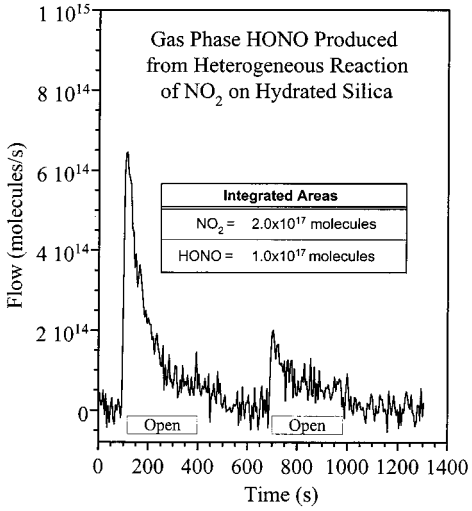

Figure 8. Flow cell reactor mass spectral data for HONO production due to heterogeneous reaction of NO_2 on hydrated SiO_2. The flow rate is shown for two gas-phase product molecules, HONO and HNO_3. The total amount of NO_2 reacted and HONO produced from heterogeneous reaction was determined, after correcting for homogeneous chemistry, from the integrated flow rate for NO_2 (using the data presented in Figure 7) and for HONO (using the data presented in this figure).

labeled hydrated. Second, the amount of adsorbed water on the hydrated sample significantly decreases as the water outgasses from the sample. Third, there is a concomitant decrease in the NO_2 uptake with the decrease in the amount of adsorbed H_2O.

The flow rate of HONO produced in the reaction is plotted in Figure 8 as a function of the reaction time. The data in Figure 8 show that HONO is immediately produced when the sample is exposed to NO_2. The amount of HONO decreases as the NO_2 uptake decreases. HNO_3 is also observed in the gas phase; this is indicative of homogeneous chemistry. The integrated areas of the molecular flow of NO_2 and HONO give the total number of molecules reacted. Because the pressure is high in the SiO_2 experiments, i.e., outside the molecular flow regime, contributions due to homogeneous chemistry have been subtracted from the data presented in Figure 8 in order to quantify the amount of HONO produced due to heterogeneous chemistry. The amount of NO_2 reacted, given in Figure 8, was obtained from the raw data presented in Figure 7 after subtraction of losses due to homogeneous chemistry. The amount of HONO formed is a factor of 2 less than the amount of NO_2 reacted (HONO/$NO_2 = 2.0$) and is consisted with the stoichiometry of reaction 3.

Atmospheric Relevance. Heterogeneous reactions of atmospheric gases on solid particles play an important role in atmospheric chemistry.[34−36] The role of surface adsorbed water in these reactions is important to our understanding of heterogeneous reaction mechanisms. For example, the chlorine activation reaction, $ClONO_2 + HCl \rightarrow HNO_3 + Cl_2$, on the surface of α-Al_2O_3 particles has been proposed to have a relatively high reaction probability of 0.02 because of a liquid water layer on the α-Al_2O_3 particles.[37] Similarly the heterogeneous reaction of HNO_3 on dried NaCl and synthetic sea salt involves the dissolution of HNO_3 in strongly adsorbed water, which is present at defect sites and as salt hydrates on the surface of these particles.[38,39]

In this study, we have demonstrated that surface adsorbed water present on SiO_2 particles can react in the presence of gas-phase NO_2 to yield surface-bound HNO_3 and gas-phase HONO according to reaction 3. Although the pressures used in this study are higher than those found in atmospheric environments, these studies clearly demonstrate that adsorbed water can participate in surface reactions and that adsorbed water is not just a medium for the adsorption and reaction of ionic species. This reaction can potentially occur on any particle surface containing surface-adsorbed water. Mineral dust particles in the atmosphere especially mineral oxide particles should have adsorbed water on the surface of these particles under atmospheric conditions and can therefore provide a reactive surface for HONO formation.

An important issue is whether HONO formation by heterogeneous reactions of NO_2 and adsorbed water sufficiently contributes to HONO concentrations found in the atmosphere. The reaction probability of the heterogeneous reaction of NO_2 and H_2O has been previously investigated and discussed. It has been concluded that the mass accommodation coefficient is the rate-limiting parameter for NO_2 uptake. The uptake coefficient of NO_2 reacting with sulfuric acid aerosols and thin films of water were measured to be near 7×10^{-6} and $<1 \times 10^{-5}$, respectively.[17] A higher uptake coefficient for NO_2 near 10^{-4} has been measured on water droplets.[40]

Other studies showed that significant amounts of HONO formed from heterogeneous reactions of NO_2 with soil[41] and cloud droplets.[42] However, Lammel and Cape have concluded that the heterogeneous rate of reaction 3 is not fast enough to explain the highest observed rates of HONO production.[12] However, a faster reaction has been observed for the heterogeneous reaction of NO_2 on soot particles.[43−45] The reaction of NO_2 on different types of soot particles has been determined. Reaction probabilities from each study were determined to be between 1.1×10^{-2} and 3.3×10^{-4},[43] and 0.12 to 0.03.[44] It should be noted that a full characterization of the products has not been made, and there is some question as to the mechanism of the soot reaction. However, a reaction is proposed that involves the production of gas-phase HONO as the sole product, i.e.,

$$NO_2(g) + H(a) \rightarrow HONO(g) \quad (5)$$

indicating that the mechanism is different from the reaction studied here.

Conclusions

Although mechanisms for HONO formation in the troposphere are not well understood, a heterogeneous, surface-catalyzed reaction of NO_2 is thought to be an important if not dominant source of HONO. Previous to this study, a full in situ characterization of the products of the reaction, $2NO_2(g) + H_2O(a) \rightarrow HONO(g) + HNO_3(a)$, had not been made. In this study, we have presented spectroscopic data that shows reaction between NO_2 and water adsorbed on a SiO_2 particle surface yields surface-bound HNO_3 and gas-phase HONO. This is the first direct evidence for the surface reaction between gas-phase NO_2 and adsorbed H_2O to yield both adsorbed and gas-phase products. Flow cell measurements show that there is also a contribution from gas-phase reactions to HONO formation.

Acknowledgment. The authors gratefully acknowledge the NSF (Grant CHE-9614134) for support of this work. G.M.U. acknowledges the Camille and Henry Dreyfus Foundation for support through the Environmental Science Postdoctoral Program.

References and Notes

(1) Chan, W. H.; Nordstrom, R. J.; Calvert, J. G.; Shaw, J. H. *Environ. Sci. Technol.* **1976**, *10*, 674.
(2) Cox, R. A. *J. Photochem.* **1984**, *25*, 43.
(3) Baulch, D. L.; Cox, R. A.; Crutzen, P. J.; Hampson, R. F.; Kerr, J. A.; Troe, J.; Watson, R. T. *J. Phys. Chem. Ref. Data* **1982**, *11*, 327.
(4) Appel, B. R.; Winer, A. M.; Tokiwa, Y.; Biermann, H. W. *Atmos. Environ.* **1990**, *3*, 611.
(5) Febo, A.; Perrino, C.; Allegrini, I. *Atmos. Environ.* **1996**, *30*, 611.
(6) Lee, Y. N.; Schwartz, S. E. *J. Geophys. Res* **1981**, *86* (11), 971.
(7) Kaiser, E. W.; Wu, C. H. *J. Phys. Chem.* **1977**, *81*, 1701.
(8) Sakamaki, F.; Hatakeyama, S.; Akimoto, H. *Int. J. Chem. Kinet.* **1983**, *15*, 1013−1029.
(9) Pitts, J. N., Jr.; Sanhueza, E.; Atkinson, R.; Carter, W. P. L.; Winer, A. M.; Harris, G. W.; Plum, C. N. *Int. J. Chem. Kinet*. **1984**, *16*, 919−939.
(10) Svensson, R.; Ljungstrom, E.; Lindqvist, O. *Atmos. Environ*. **1987**, *21*, 1529.
(11) Jenkin, M. E.; Cox, R. A.; Williams, D. J. *Atmos. Environ.* **1988**, *22* (13), 487.
(12) Lammel, G.; Cape, J. N. *Chem. Soc. Rev.* **1996**, 361.
(13) Junkermann, W.; Ibusuki, T. *Atmos. Environ* **1992**, *26A* (17), 3099.
(14) Notholt, J.; Hjorth, J.; Raes, F. *Atmos. Environ* **1992**, *26*, 211.
(15) Becker, K. H.; Kleffmann, J.; Kurtenbach, R. *J. Phys. Chem.* **1996**, *100*, 14984.
(16) Harrison, R. M.; Peak, J. D.; Collins, G. M. *J. Geophys. Res* **1996**, *101*, 14429.
(17) Kleffmann, J.; Becker, K. H.; Wiesen, P. *Atmos. Environ* **1998**, *32* (16), 2721.
(18) Finlayson-Pitts, B. J.; Pitts, J. N., Jr. *Atmospheric Chemistry: Fundamentals and Experimental Techniques*; John Wiley & Sons: New York, 1986; p 540.
(19) Febo, A.; Perrino, C. *Atmos. Environ*. **1991**, *25A*, 1055.
(20) Tabazadeh, A.; Jacobson, M. Z.; Singh, H. B.; Toon, O. B.; Lin, J. S.; Chatfield, R. B.; Thakur, A. N.; Talbot, R. W.; Dibb, J. E. *Geophys. Res. Lett*. **1998**, *25*, 4185.
(21) Dentener, F. J.; Carmichael, G. R.; Zhang, Y.; Lelieveld, J.; Crutzen, P. J. *J. Geophys. Res.* **1996**, *101*, 22869.
(22) Zhang, Y.; Sunwoo, Y.; Kotamarthi, V.; Carmichael, G. *J. Appl. Meteorol.* **1994**, *33*, 813−824.
(23) Goodman, A. L.; Miller, T. M.; Grassian, V. H. *J. Vac. Sci. Technol. A* **1998**, *16*, 2585.
(24) Miller, T. M.; Grassian, V. H. *Geophys. Res. Lett*. **1998**, *25*, 3835.
(25) Underwood, G. M.; Miller, T. M.; Grassian, V. H. *J. Phys. Chem. A* **1999**, *103*, 6184.
(26) Little, L. H. *Infrared Spectra of Adsorbed Species*; Academic Press: London, 1966.
(27) Sneh, O.; Cameron, M. A.; George, S. M. *Surf. Sci.* **1996**, *364*, 61.
(28) Shimanouchi, T. *J. Phys. Chem. Ref. Data* **1977**, *6*, 1039.
(29) Leuchs, M.; Zundel, G. *J. Phys. Chem.* **1978**, *82*, 1632.
(30) Jacox, M. E. *J. Phys. Chem. Ref. Data* **1984**, *13*, 945.
(31) Jacox, M. E. *J. Phys. Chem. Ref. Data* **1990**, *19*, 1444.
(32) The HNO_3 parent ion mass spectrometer signal was calibrated and converted to flow using an authentic sample of HNO_3. There is no readily available source of pure gaseous HONO and therefore mass spectral calibration of this species is more difficult. The NO^+ ion signal, $m/e = 30$, has three contributions, mass spectral fragmentation of NO_2, HNO_3, and HONO. Since the HNO_3 and NO_2 contributions to the NO^+ ion signal and the overall NO^+ ion signal are known, the HONO contribution can be determined. If it is assumed that the throughput of NO^+ through the spectrometer is independent of its source, then the number of NO^+ ions from HONO can be determined. From this, the parent ion, $m/e = 47$, signal is calibrated to flow rate (after contributions from $^{15}NO_2$ are first subtracted out) from the HONO contribution to the NO signal and the mass spectral fragmentation of HONO taken from ref 33.
(33) Fenter, F. F.; Caloz, F.; Rossi, M. J. *J. Phys. Chem.* **1996**, *100*, 1008.
(34) Andreae, M. O.; Crutzen, P. J. *Science* **1997**, *276*, 1052.
(35) Finlayson-Pitts, B. J.; Pitts, J. N., Jr. *Science* **1997**, *276*, 1045.
(36) Ravishankara, A. R. *Science* **1997**, *276*, 1058.
(37) Molina, M. J.; Molina, L. T.; Zhang, R.; Meads, R. F.; Spencer, D. D. *Geophys. Res. Lett.* **1997**, *24*, 1619.
(38) Beichert, P.; Finlayson-Pitts, B. J. *J. Phys. Chem.* **1996**, *100*, 15218.
(39) De Haan, D. O.; Finlayson-Pitts, B. J. *J. Phys. Chem. A* **1997**, *101*, 9993.
(40) Mertes, S.; Wahner, A. *J. Phys. Chem.* **1995**, *99*, 14000.
(41) Harrison, R. M.; Kitto, A. M. N. *Atmos. Environ.* **1994**, *28*, 1089.
(42) Lammel, G.; Perner, D. *J. Aerosol. Sci* **1988**, *19*, 1199.
(43) Ammann, M.; Kalberer, M.; Jost, D. T.; Tobler, L.; Rossler, E.; Piguet, D.; Gaggeler, H. W.; Baltensperger, U. *Nature* **1998**, *395*, 157.
(44) Gerecke, A.; Thielmann, A.; Gutzwiller, L.; Rossi, M. J. *Geophys. Res. Lett*. **1998**, *25*, 2453.
(45) Longfellow, C. A.; Ravishankara, A. R.; Hanson, D. R. *J. Geophys. Res.* **1999**, *104*, 13833.